1.7. Purpose

Thus, nanosizing effect is involved with plural processes and sometimes causes different behaviour from macroscopic size to biocompatible materials. This strongly suggests the necessity to reveal the micro/nanosizing effect of materials on the living organism. The present paper discusses the bioreaction of nanoparticles based on reviewing authors' past and additional data, where both biochemical cell functional tests and animal implantation tests investigated the micro/nanosizing effect and the dependence particle size on the reaction of cells and tissues. The behaviour of invading nanoparticles and internal diffusion inside the body was visualized using X-ray scanning analytical microscope (XSAM; Uo *et al.* 1999, 2001*a*,*b*, 2006) for the level of the whole body and organs (Watari *et al.* 2007*c*,*d*, 2008*a*). Then, the nanosizing effect on tissue regeneration and cell proliferation in apatite and CNTs was investigated, and the mechanism of the conversion of functions from those in macroscopic scale was discussed.

2. MATERIAL AND METHODS

2.1. Specimens

Various sizes of particles were used as specimens for 99.9 per cent pure Ti, Fe, Ni, TiO_2 and CNTs. For Ti and Fe, particles of nominal size from 500 nm to 150 μm were used. To reduce the size distribution as small as possible and equalize the experimental conditions among the materials of metallic Ti, Fe and Ni, the particles of 500 nm, 3 and 10 μm were extracted by sedimentation and those less than 300 nm were extracted by ultrafiltration from the particle group with the size distribution (Tamura, K. *et al.* 2002).

2.2. Dissolution test of Ti, Fe and Ni particles

After Ti, Fe and Ni particles were immersed in Hanks balanced salt solution (HBSS) at 37°C for one month, the supernatant was filtered through a 0.45 μm membrane to remove particles and then elemental analysis was done by inductively coupled plasma-atomic emission spectrometry (ICP-AES) using ICPS-8100, Shimazu, Tokyo, Japan.

2.3. Biochemical analyses of cellular reaction to materials

Particles smaller (500 nm and 3 μm) and larger (10, 50 and 150 μm) than neutrophils were used to determine the relationship between cells and particle size with respect to cytotoxicity.

Human neutrophils, which play a central role in the initial stage of inflammation against foreign bodies, were used as probe cells. Neutrophils were separated from human peripheral blood from healthy volunteers with 6 per cent isotonic sodium chloride containing the hydroxyethyl starch and lymphocyte isolation solution (Ficoll-Hypaque, Amersham Pharmacia Biotech AB, Sweden). After the particles were mixed with HBSS kept at 37°C and neutrophils were added, they were used for various cell toxicity tests. The human acute monocytic leukaemia cell line, THP-1 cell, was also used for additional experiments.

Cell survival rate, lactate dehydrogenase (LDH) values and superoxide anion (O^{2-}) production per 10^6 neutrophils were measured. Cytokines of tumor necrosis factor-α (TNF-α) and interleukin-1β (IL-1β) were measured using ELISA kits (Endogen, Inc. USA). Morphological change of neutrophils mixed with HBSS containing various particles was observed by optical microscopy (OM: Zeiss, Axioskop, Germany) and scanning electron microscopy (SEM: Hitachi S-4300, Tokyo, Japan) (Kumazawa *et al.* 2002; Tamura, K. *et al.* 2002).

2.4. Animal implantation experiments

Particles were inserted into the subcutaneous connective tissue in the abdominal region of Wistar rats aged between 11 and 12 weeks (weight 350–380 gf). Specimens were prepared through the usual process of fixation, embedding, sectioning, staining with haematoxylin–eosin and histopathological observation was performed.

2.5. Visualization of internal distribution of nanoparticles

The compulsory exposure test to the respiratory system was performed on rats using the TiO_2 particles of a nominal size 30 nm. The uptake of nanoparticles through the digestive system was also tested in mice by mixing agar gelatin containing 30 nm TiO_2 particles with their foods. To inspect internal diffusion more simply, the experiments were done for mice by injecting nanoparticles directly into the cardiovascular system to the caudal vein. The observation of the internal distribution of nanoparticles was conducted for the whole body and each organ by elemental mapping in air using XSAM (Horiba XGT-2000V, Tokyo, Japan) without the pre-treatments of fixation, dehydration and staining after sectioning. The distribution inside the organ was also inspected by elemental mapping using energy dispersive X-ray spectroscopy (EDS) installed to SEM. The experiments were also carried out for the particles Ti, Fe, Ni, Pt, TiO_2, TiC, Fe_3O_4, Fe_2O_3 and CNTs. Chemical analysis was done by ICP-AES for organs and compared with the results of XSAM mapping (Watari *et al.* 2007*c*,*d*, 2008*a*).

2.6. Biomimetic nanoapatite/collagen composite

HAP–collagen composites synthesized biomimetically on collagen type I were implanted into the subcutaneous tissue and bone defects in the femur of rats for 1–12 weeks and observed histopathologically (Yokoyama *et al.* 2005*b*).

2.7. CNTs

CNTs were used including single-wall CNTs (SWCNTs) of 0.9–1.5 nm in diameter and 2–3 μm in

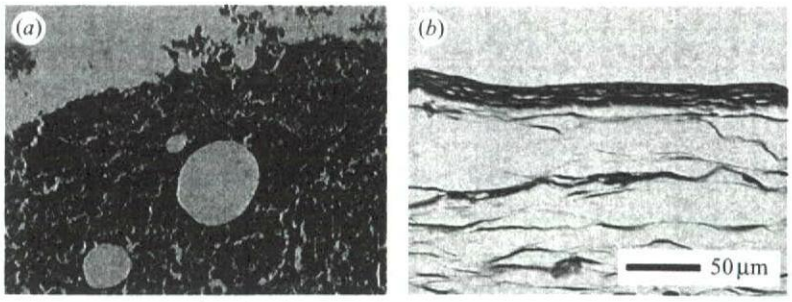

Figure 2. Histological image of rat soft tissue inserted with (*a*) Ni and (*b*) Ti implants of macroscopic size (1 mm $\phi \times 10$ mm) after one week (Watari *et al.* 2007*b*).

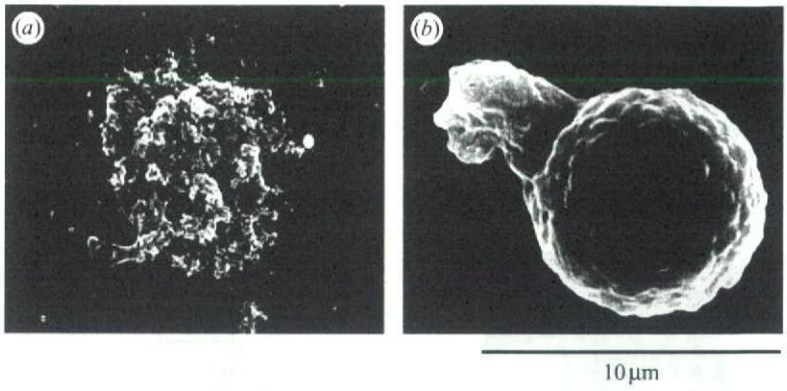

Figure 3. SEM images of human neutrophils exposed to the 500 nm particles of (*a*) Ni and (*b*) Ti (Watari *et al.* 2007*b*).

length synthesized by arc discharge method with a purity of 90 per cent (Meijo Nano Carbon Co., Ltd), multi-wall CNTs (MWCNT) of 5–20 nm in diameter and 20–40 μm in length synthesized by the chemical vapour deposition technique with a purity of 98 per cent (NanoLab, Inc., MA, USA) and carbon nanofibres for part of the experiments. In some cases, CNTs were purified by the removal of metal particle catalysts of Ni and Fe using acid agents such as hydrochloric acid and amorphous carbon by heating in air. By these treatments, CNTs gained some hydrophilicity. CNTs were dispersed in the deionized water by sonication for 3 min. Various nanotube (NT) scaffolds were made by vacuum filtration of the dispersed NT slurry onto porous polycarbonate (PC) membranes.

2.8. Cell culture

Human osteoblast-like cells (Saos2) were used for cell culture. Cells were cultured in Dulbecco's modified Eagle's medium (DMEM; SIGMA) with 10 per cent foetal bovine serum (FBS; Biowest) by the usual process. The morphology of cells was observed by OM, confocal laser scanning microscopy and SEM. The number of cells was counted from the SEM micrographs of those attached to each scaffold, since the detachment of cells from scaffold by trypsin could not be applied for CNT scaffolds. The adsorbed amount of proteins on each scaffold was measured using bicinchoninic acid protein assay reagent after immersion in the cell culture medium for 24 hours. Alkaline phosphatase (ALP) activity was measured with LabAssay ALP (Wako, Japan) for the cells cultured on each scaffold (Aoki *et al.* 2005, 2006, 2007*a*,*b*).

2.9. Observation and characterization

Morphology of particles and cells was observed by SEM, and elemental analysis by EDS was also carried out. The high resolution observation of CNT was done with the multi-beam high-voltage electron microscope (JEM-ARM-1300, JEOL, Japan) of the Center for Advanced Research of Energy Conversion Materials, Hokkaido University, at an accelerating voltage of 1250 kV.

Animal experiments were performed in accordance with the Guide for the Care and Use of Laboratory Animals, Hokkaido University Graduate School of Dental Medicine. During the course of this study, no rats were lost.

3. RESULTS

3.1. Soluble and non-soluble materials: reaction from macro to micro/nano

Figure 2 shows the comparison of tissue reaction to the macroscopic size (1 mm $\phi \times 10$ mm) of Ni (figure 2*a*) and Ti (figure 2*b*) after one week implantation in the dorsal thoracic region of rat. The implant had been situated in the upper space of each photograph. In Ni, the expansion of capillary vessels was observed. Tissue in the photograph was showed necrosis and degeneration in the distant region. For Ti, a fibrous connective tissue had already formed surrounding implants from the earlier stage, which is a feature of biocompatible materials.

Figure 3 shows the SEM image of human neutrophils exposed to the 500 nm particles of Ni (figure 3*a*) and Ti (figure 3*b*) in HBSS. The morphology of neutrophils exposed to Ni particles was often transformed or

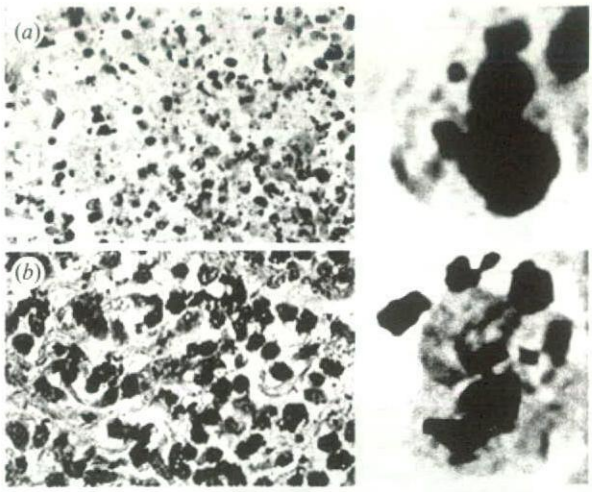

Figure 4. Histopathological observation of tissue reaction to the short-term implantation of the (*a*) 500 nm Ni and (*b*) 3 μm Ti particles. The enlargement of one cell is shown on the right. (*a*) Necrosis and (*b*) inflammation occurred, respectively.

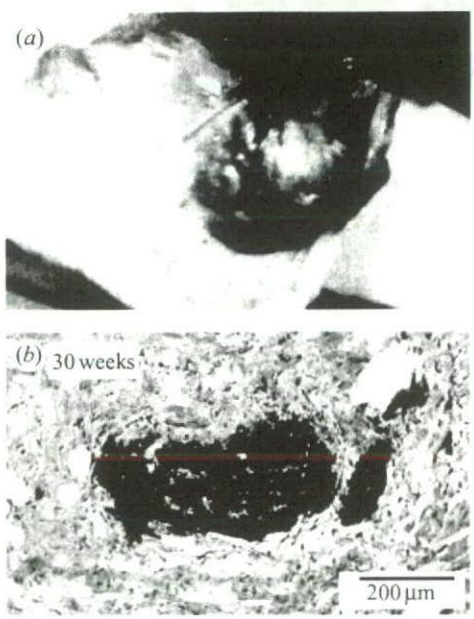

Figure 5. Tissue reaction for the long-term implantation to the (*a*) 500 nm Ni and (*b*) 3 μm Ti particles. Tumour was induced after 1 year implantation of the 500 nm Ni particles (Watari *et al.* 2007*b*).

destroyed due to its toxicity (figure 2*a*). For Ti (figure 2*b*), a neutrophil is extending its pseudopod and going to phagocytize a 500 nm Ti particle. For the particles larger than approximately 10 μm, phagocytosis was not observed.

Figure 4 shows the comparison of histopathological observation of tissue reaction to the short-term (5 days) implantation in the subcutaneous tissue of the rat for 500 nm Ni and 3 μm Ti particles. The enlargement of a single cell is shown on the right side. For Ni particles necrosis occurred, while Ti particles were phagocytized by macrophages and other giant cells.

Figure 5 showed the tissue reaction to the long-term implantation of the 500 nm Ni and 3 μm Ti particles. Figure 5*a* is a tumour induced after a 1-year implantation

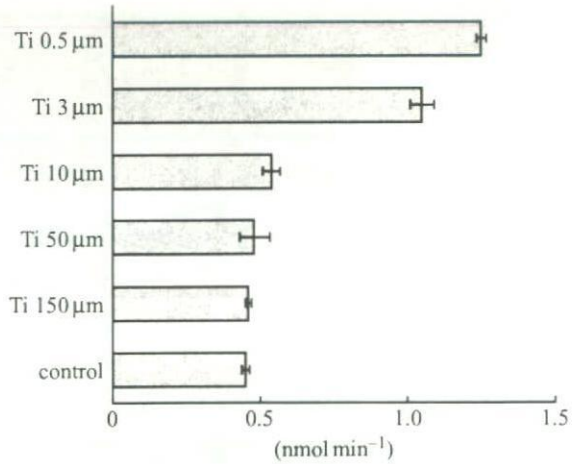

Figure 6. Dependence of superoxide production from neutrophils on Ti particle size (Tamura, K. *et al.* 2002).

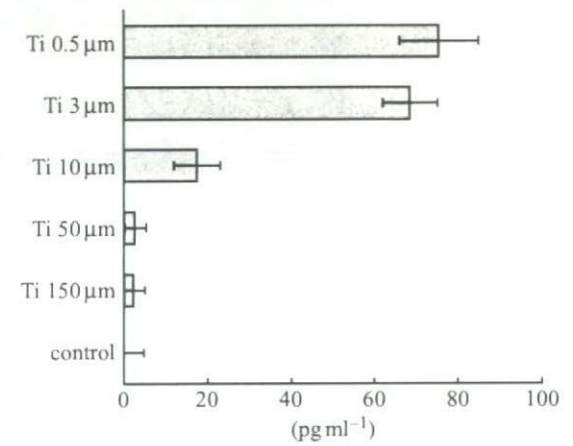

Figure 7. Dependence of IL-1β production from neutrophils on Ti particle size (Tamura, K. *et al.* 2002).

of Ni particles in the subcutaneous tissue of a rat. Ni is already toxic in macroscopic size as seen in figure 2. When fine particles, toxicity is enhanced remarkably. Figure 5*b* shows 3 μm Ti particles after 30 weeks. Particles had been dispersed more widely in tissue just after implantation. In the long term, they became gradually agglomerated by the biological processes of repeated cycles of phagocytosis and cell death.

3.2. *Particle size dependence on cell/tissue reaction and function*

Figures 6 and 7 show the released amount of superoxide and IL-1β from human neutrophils in HBSS mixed with the various sizes of Ti particles. IL-1β is one of the most representative cytokines of inflammation. HBSS was the control. Both superoxide and IL-1β were increased with the decrease in particle size. The increase was especially pronounced for 3 μm and 500 nm. The release of LDH showed similar behaviour, while cell survival rate showed the inverse decreasing tendency.

Figure 8 shows the dissolution from 3 and 10 μm particles of Ti (figure 8*a*), Fe (figure 8*b*) and Ni (figure 8*c*) analysed by ICP-AES. Under the conditions of figures 6 and 7, ICP elemental analysis indicated that the dissolution from Ti particles was

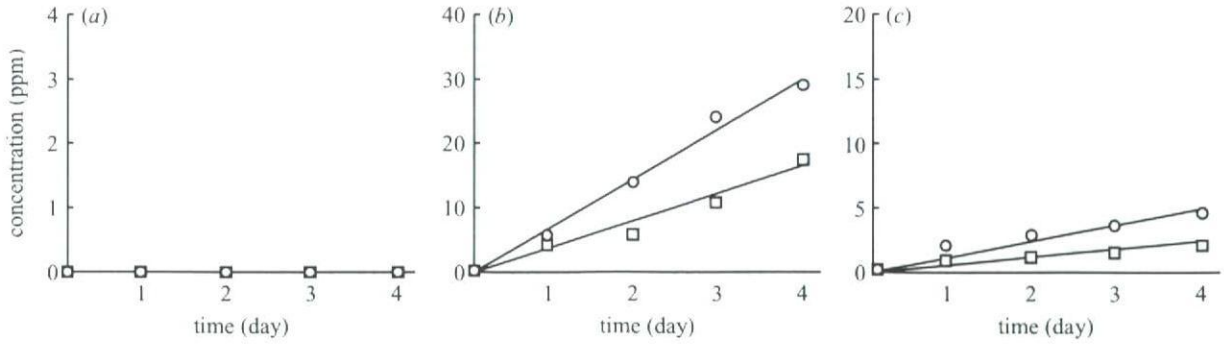

Figure 8. Dissolution from 3 μm (circles) and 10 μm (squares) particles of (*a*) Ti, (*b*) Fe and (*c*) Ni analysed by ICP-AES.

negligible below detection limit. This suggests that the pronounced phenomena of biochemical cell reaction seen below 10 μm in figures 6 and 7 are not due to the ionic dissolution effect.

For Fe and Ni, the dissolution amount depends on the particle size. The smaller 3 μm particles dissolve more than 10 μm particles. Fe is very soluble if we take the 10 times larger value of the vertical axis into account. The dissolution of Ni is smaller than Fe, but Ni shows a much more toxic effect as shown in figures 2–5.

Figure 9 shows the comparison of TNF-α release for Ti, Fe and Ni particles. TNF-α is another one of the most representative cytokines of inflammation as well as IL-1β. Ti and Fe showed the similar increasing tendency with the decrease in particle size. The increase was drastically pronounced for 3 μm particles. ICP results (figure 8) showed that the chemical properties of Ti and Fe particles are completely different. Ti is non-soluble and Fe is very soluble. Nevertheless, the effect of Fe is nearly equivalent to that of Ti even in a quantitative sense, although the chemical properties of each are very different.

Ni also showed the size dependence. However, the quantitative values are different from Ti and Fe. Ni showed the size dependence with the relatively lower values. The release of superoxide and IL-1β showed a tendency similar to that for Ti and Fe. Cell survival rate was much smaller than control (HBSS) and LDH was higher.

Figure 10 shows the histological image of rat tissue reaction to 3 μm (figure 10*a*) and 10 μm (figure 10*b*) Ti particles after 5 days of implantation in the soft tissue of rat. For the 3 μm Ti particles, phagocytosis by macrophages and inflammatory cells occurred, and Ti particles were observed in the cytoplasm of cells, whereas the 10 μm Ti particles were outside cells, phagocytosis was rarely observed and tissue was much less inflammatory. The size dependence *in vivo* observed in figure 10 resembles the results *in vitro* in figures 3*b* and 9, which suggests that TNF-α expression is closely related to the occurrence of phagocytosis.

The histological observation of rat tissue reaction to the implantation of different size of Ti particles 3, 10, 50 and 150 μm was carried out for up to 30 weeks. For the 150 μm Ti, each particle was surrounded by fibrous connective tissue layer, which is similar to the case of macroscopic Ti implant shown in figure 2*b*. Tissue reaction to the 10 μm Ti was inflammatory with inflammatory cell infiltration as well as fibrous

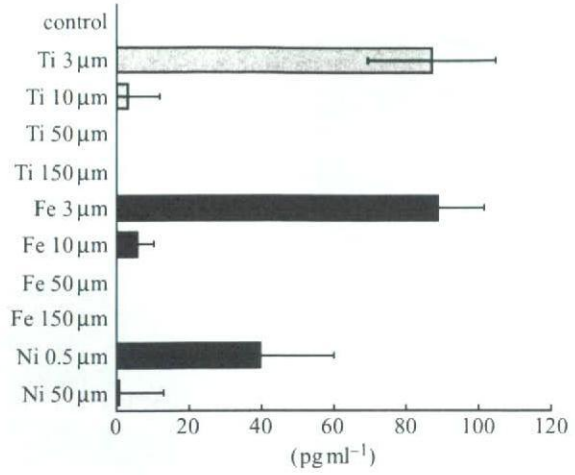

Figure 9. Dependence of TNF-α release from neutrophils on particle size for Ti, Fe and Ni (Watari *et al.* 2007*a*).

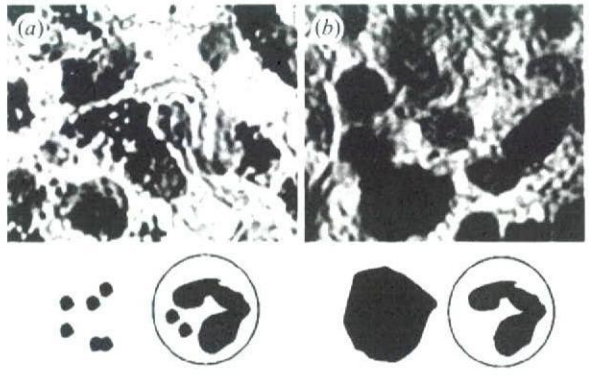

Figure 10. Tissue reaction of rat to (*a*) 3 μm and (*b*) 10 μm Ti particles after 5 day implantation (Watari *et al.* 2007*a*).

connective tissue formation. For the 3 μm Ti, the originally dispersed particles in tissue in short-term implantation became gradually agglomerated over time in the long term by the biological process of repeated cycles of phagocytosis and cell death. Weak inflammation continues chronically after 30 weeks.

3.3. *Invasion and internal diffusion of nanoparticles*

Figure 11 shows the dependence of TNF-α release from neutrophils on particle size down to the nm scale. Stimulus, represented as amount of TNF-α release, is

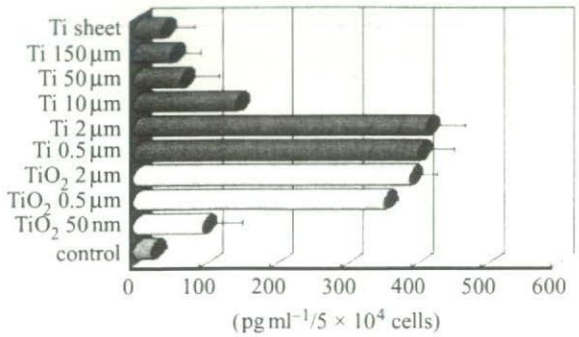

Figure 11. Dependence of TNF-α release from neutrophils on particle size down to the nm scale (Watari *et al.* 2007*a*).

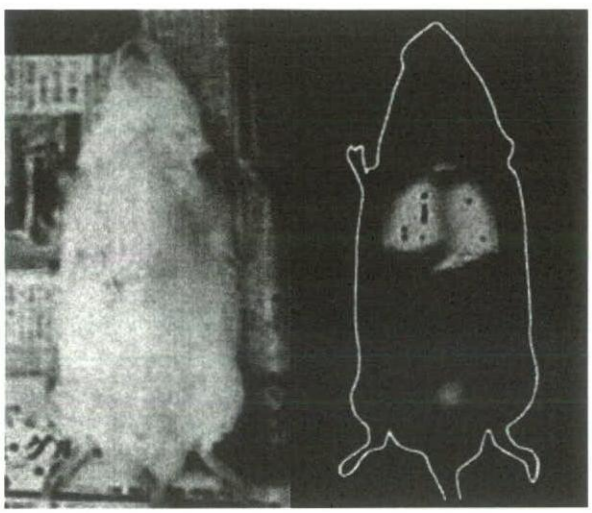

Figure 12. XSAM Ti mapping of internal distribution of the 30 nm TiO_2 particles after the compulsory exposure testing of the respiratory system (Watari *et al.* 2007*d*).

pronounced below 3 μm. It exhibited the maximum from approximately μm down to 500 nm. For smaller sizes, it decreased below 200 nm and became closer to the level of 50 μm and larger.

Figure 12 is the Ti mapping of the internal whole body of rats by XSAM after a compulsory exposure test. It shows the distribution of the 30 nm TiO_2 particles. The condensation occurred from the respiratory system to urinary bladder by diffusion in the whole body through the cardiovascular system after the direct uptake from pulmonary alveoli into blood vessels.

Figure 13 is the XSAM elemental analysis from the spleen for the case after 10 days of oral administration of 30 nm TiO_2 particles. Although peak height is small in this case, a Ti-Kα peak undoubtedly exists other than Fe-Kα peaks at approximately 6.5 keV and peaks of incident X-ray from Rh target below 4 keV. This confirms the phenomenon that nanoparticles were taken into the internal body through the digestion system.

Figure 14 shows the X-ray transmission image and the corresponding Ti elemental mapping by XSAM for 5 min, 3 hours and 1 day after injection of the 30 nm TiO_2 particles directly into the cardiovascular system of the mouse through the caudal vein. TiO_2 nanoparticles diffuse to the lung through the heart

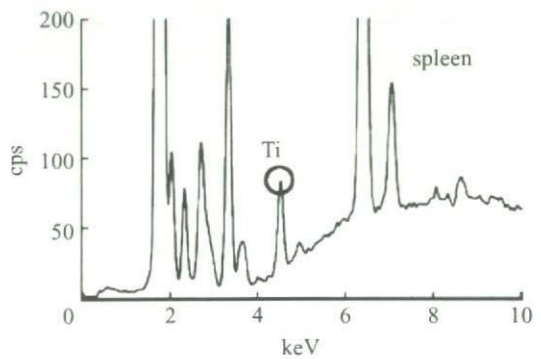

Figure 13. Elemental analysis of spleen of mouse by XSAM after oral administration of 30 nm TiO_2 particles for 10 days (Watari *et al.* 2008*a*).

from the caudal vein just after injection, then to the liver and further to the spleen with time.

3.4. Conversion of functions by nanosizing and HAP

Figure 15 shows an example of failure in a dental implant of HAP-coated titanium before (figure 15*a*) and after (figure 15*b*) implantation. Failures of dental implant occur for various reasons. One of the causes is the dust of apatite produced by dropout, exfoliation, delamination or abrasion. This induces inflammation and the resorption of newly formed bone and coated apatite.

The biomimetically synthesized nanocomposites of apatite and collagen fibrils are bioresorbable in the subcutaneous tissue. Then these nanoapatite composites were implanted in bone defects or bone marrow. Figure 16 shows the histopathological image when nanoapatite composites were implanted in the bone marrow of rat for eight weeks. Phagocytosis of composites by osteoclasts and osteogenesis by osteoblasts occurred simultaneously and adjacently to each other. The area of nanocomposites (asterisks) was decreased and covered with new bone (white asterisks) of lamellar structures. Resorption of the composites and replacement by new bone proceeded with time by 12 weeks. As a result, nanoapatite composites work as bone substitute materials for hard-tissue reconstruction.

3.5. Conversion of functions by nanosizing CNTs

Figure 17 shows the SEM image of osteoblast-like Saos2 cells cultured on graphite (figure 17*a*) and MWCNT (figure 17*b*) scaffolds for 7 days. Although graphite and CNTs are isomorphs of carbon and composed of graphene sheets that are similarly in crystal structure, they make a contrasting difference in the cell attachment and proliferation. Very few cells were attached to graphite (figure 17*a*), while many cells were attached to CNTs (figure 17*b*).

Cell growth cultured on CNTs showed the characteristic behaviour. Saos2 is usually grown in a spindle shape. On CNT scaffold, cells are grown fully to the whole direction with numerous fine filopodia at the cell edge.

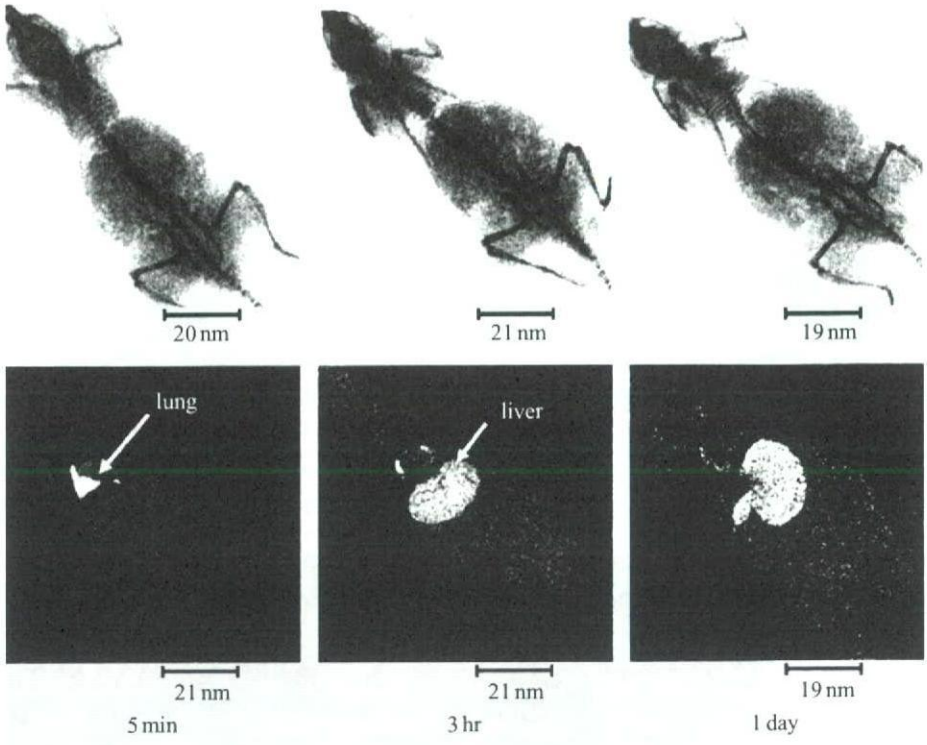

Figure 14. Time course of internal diffusion of the 30 nm TiO_2 particles after injection to the caudal vein, visualized by XSAM.

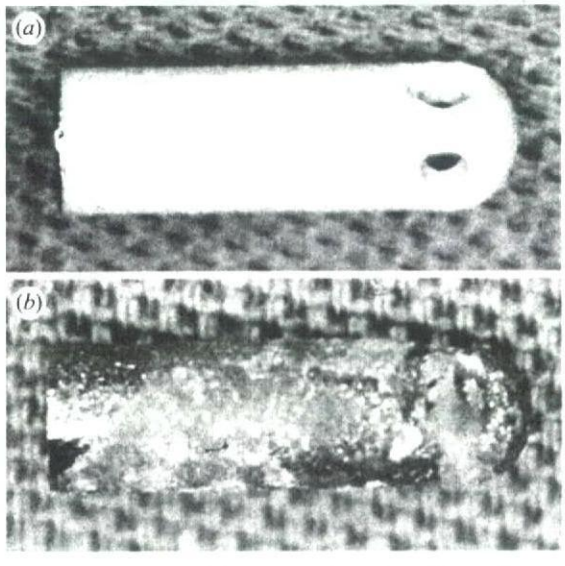

Figure 15. Example of failure in dental implant of apatite-coated titanium: (*a*) before and (*b*) after implantation.

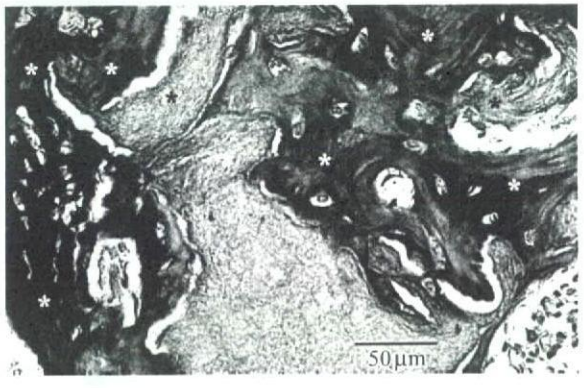

Figure 16. Histological image at eight weeks after implantation in the bone marrow of rat. Nanocomposites were resorbed (black asterisks) and partly replaced by new bone (white asterisks) with lamellar structures. AZ stain.

Figure 18 shows the SEM observation of the filopodia grown from the periphery of osteoblast-like cells on MWCNT scaffolds (figure 18*a*) and the enlarged image of the end of filopodium (figure 18*b*). Compared with usual cell culture, numerous filopodia are extended farther in the cell periphery (figure 18*a*) and combined with CNT meshwork. When trypsin, usually used to detach cells for cell number counting, was applied, cells would normally detach and float up, but could not separate from scaffold owing to the binding of filopodia with CNTs. These results show the high cell adhesiveness of CNTs.

Figure 19 shows the number of Saos2 cells cultured on the scaffolds of PC, graphite, MWCNT and SWCNT for 7 days. The cell numbers increased with culture time. However, cell number was nearly null on graphite, and the largest on SWCNTs of the four scaffolds, followed by MWCNTs.

Figure 20 shows the adsorbed amount of proteins on the scaffolds of PC, graphite, MWCNT and SWCNT when immersed in the cell culture medium for 24 hours. The amount of adsorbed protein is very low for graphite and the highest for SWCNT, followed by MWCNT.

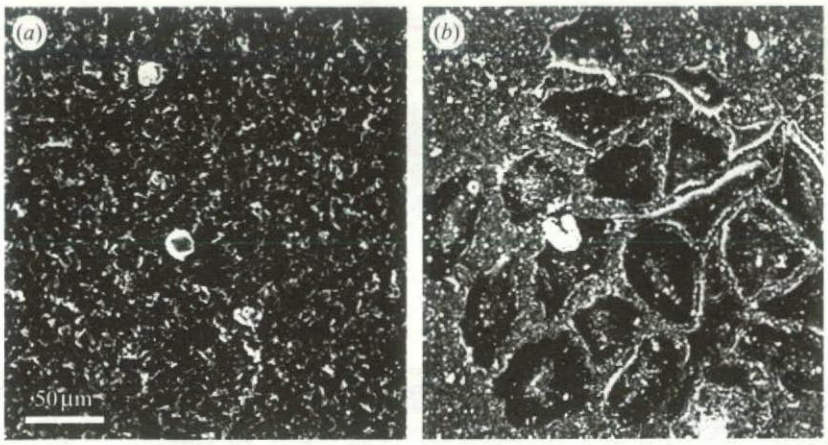

Figure 17. SEM image of osteoblast-like Saos2 cells cultured on (*a*) graphite and (*b*) MWCNT scaffolds for 7 days.

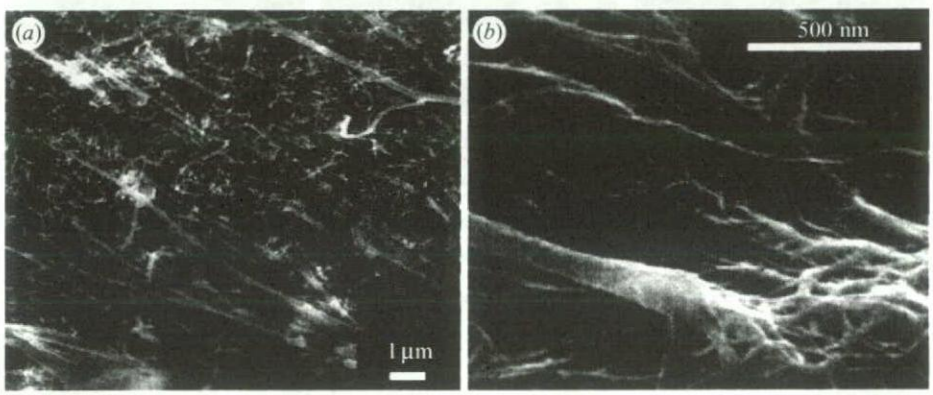

Figure 18. (*a*) SEM observation of filopodia grown from the periphery of osteoblast-like cells on MWCNT scaffolds and (*b*) the enlarged image of the end of filopodium.

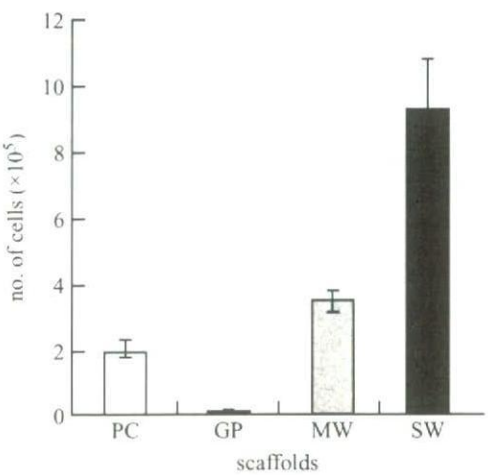

Figure 19. Number of Saos2 cells cultured on the scaffolds of PC, graphite (GP), MWCNT (MW) and SWCNT (SW) for 7 days.

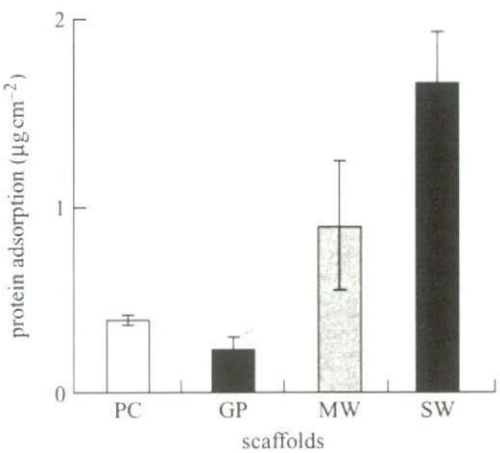

Figure 20. Adsorbed amount of proteins on the scaffolds of PC, graphite (GP), MWCNT (MW) and SWCNT (SW) in cell culture medium after 24 hours immersion (Aoki *et al.* 2007*a*).

Figure 21 is the expression of normalized ALP activity from osteoblast-like cells (Saos2) cultured on scaffolds of PC, graphite, MWCNT and SWCNT for 7 days. The degree of expression was very low for graphite, while it was increased remarkably in CNTs, the greatest increase in SWCNTs, then MWCNTs.

4. DISCUSSION

4.1. Soluble and non-soluble materials: effect on biocompatibility in macroscopic size

One of the most influential factors on biocompatibility of materials (Matsuno *et al.* 2001) is their dissolution

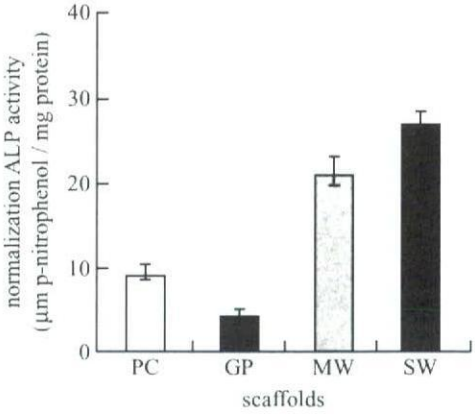

Figure 21. Expression of normalized ALP activity from Saos2 cells cultured on the scaffolds of PC, graphite (GP), MWCNT (MW) and SWCNT (SW) for 7 days.

properties. The interaction of materials with cells and tissue starts in most cases from ionic dissolution, whether it is nutrition intake or toxicity expression by poison. The toxicity effect may be evaluated as the degree of toxicity of materials×solubility. Corrosion resistance is, therefore, a prerequisite for biomaterials. This is the case for most of materials in a macroscopic size.

To compare the dependence of reaction of cells and tissue on the properties of materials with and without dissolution, Ni and Ti were selected as the representative metals for dissolvable, toxic metals and for non-dissolvable, biocompatible metals, respectively. Figures 2–5 showed the change of bioreaction to materials for the size from macroscopic to micro/nanometre. For macroscopic size, Ni (figure 2*a*) showed necrosis in the surrounding tissue of implant, while Ti (figure 2*b*) is encapsulated with fibrous connective tissue, which is the typical reaction of tissue to biocompatible materials (Uo *et al.* 2001*a*,*b*).

4.2. Nanosizing effect: specific surface area effect, the contribution of composition

The specific surface area increases in a reciprocally proportional manner to particle size. Therefore, the importance of dissolution properties becomes greater for micro- and nanosizes (downward direction in figure 1*a*) where the increase in specific surface area by nanosizing increases further chemical reaction, functions and toxicity. As shown in the *in vitro* cell reaction of figure 3, Ni caused the destruction of cells (neutrophils) (figure 3*a*) and Ti induced phagocytosis (figure 3*b*), when the size of materials became micro/nanometre (submicron).

As to the material dependence of cell toxicity that is, in other words, the effect of composition, the reaction similar to figure 3 *in vitro* also occurs *in vivo* as seen in figure 4 where necrosis occurred in cells and tissue for Ni nanometric particles. The results of figure 4 are those for the short term. The long-term implantation in tissue shown in figure 5 revealed that Ni particles generated a tumour after 1 year. This is the typical example of the specific surface area effect that leads to the enhancement of chemical dissolution and therefore toxicity. It has a serious influence, causing toxicity in many cases and is most commonly taken into account for nanosizing effect.

4.3. Nanosizing effect: physical size effect

For biocompatible materials such as Ti and TiO_2, particles below 10 μm cause phagocytosis to cells as shown *in vitro* to neutrophils (figure 3) and *in vivo* to macrophages mostly (figure 4), and weak inflammation to tissue in the short term (figure 4). For the particles larger than approximately 10 μm, phagocytosis was not observed. A similar phenomenon of size dependency was also observed *in vivo* as shown in figure 10 where the 3 μm Ti particles were phagocytized by macrophages or giant cells, while the 10 μm Ti particles remained outside the cells, phagocytosis was rarely observed and tissue was much less inflammed. In the long term (figure 5), the originally dispersed 3 μm particles were agglomerated after multiple repetitions of phagocytosis and cell death for 30 weeks. Tissue remained in a light chronic inflammation state.

This effect involved the biological reaction process between particles and cells/tissues (figure 1*b*), which is different from the case of Ni. These phenomena cannot be explained by the specific surface area effect (figure 1*a*), but understood as the different effect from the material properties of either toxicity or biocompatibility. It is the physical size and shape effect. To see the further details of this effect, *in vitro* biochemical cell functional testing was performed.

4.4. Particle size dependence in cell functions

Superoxide anions are released from intracellular organs and cell membranes when cells are stimulated. TNF-α and IL-1β are the representative cytokines of inflammation.

The production of superoxide anion (figure 6), cytokines IL-1β (figure 7) and TNF-α (figures 9 and 11) showed an increasing tendency with an decrease in particle size, and the amount was pronounced remarkably with 500 nm and 3 μm particles. SEM and OM observations (figures 3 and 10) showed that only the 500 nm and 3 μm particles in Ti group were phagocytized by neutrophils. Phagocytosis is difficult for the particle sizes 10, 50 and 150 μm to neutrophils of approximately 5–10 μm in diameter.

Similarly, the cell survival rate decreased and, with a strong corresponding relationship, the value of LDH, which is the indication of cell disruption, increased, as the particle size of Ti decreased from 150 μm down to 500 nm (Kumazawa *et al.* 2002; Tamura, K. *et al.* 2002).

All the results showed agreement in their size dependence and the size effect becomes more remarkable with a decrease in size and especially pronounced for sizes below cell size, which is closely related to the phagocytosis shown in figures 3 and 10.

ICP elemental analysis showed that the dissolution from Ti particles was below the detection limit and negligible (figure 8). Therefore, the biofunctional change detected in the present study did not result

from a chemical effect of Ti ions, but occurred by physical size effect of Ti particles.

Another evidence for physical effect is the particle size dependence of TNF-α for different materials, Ti and Fe, which are biocompatible or cause very little cell toxicity in the macroscopic size. Although the chemical properties are quite different, Ti is insoluble and Fe is soluble as shown in the ICP elemental analysis (figure 8), figure 9 showed nearly the same size dependency of TNF-α emission even in a quantitative sense. This indifference in cytotoxicity between Ti and Fe again strongly suggests that cytotoxicity of these Ti and Fe particles is not due to the chemical effect by dissolved ions but the physical size effect. Further study using other materials such as ceramics (TiO_2) and polymer (polylactic acid; PLA) showed similar particle size dependence, which suggests that these phenomena observed in biocompatible or bioinert materials are the non-specific, physical particle and shape effects, which occur independently of materials.

4.5. Critical size from bulk to particles for biological organisms

Our past *in vivo* implantation tests in the soft tissue of rats using various sizes of Ti particles showed that the particles larger than 150 μm were each surrounded by fibrous connective tissue and there was no inflammation (Kumazawa *et al.* 2002). This is the usual reaction for the biocompatible materials of a macroscopic size such as the bulk Ti implant. For less than 100 μm, the cell becomes stimulated gradually by the decrease in particle size, partly because of the mechanical and morphological factors such as irritation by needlepoint shape crystals or acute surface roughness structure onto the cell wall. It is partly the effect of IL-1β sensitivity to particle shape as discussed below in §4.6. Another reason may be that the size becomes too small to encapsulate each particle with fibrous connective tissue, and particles tend to be exposed directly to cells/tissue. Thus, for biological bodies, the object approximately larger than 100 μm behaves as macroscopic or non-bioreactive and that less than approximately 100 μm behaves as particles.

4.6. Particle shape effect

TNF-α and IL-1β are both representative cytokines of inflammation. Our past study compared the effect of different particle morphology on the expression of TNF-α and IL-1β, using the set of massive and acicular TiO_2 particles with the equivalent diametral size and longitudinal length of 3–10 μm, respectively. TNF-α showed the increase in emission below 10 μm in a similar manner for both massive and acicular crystals. For IL-1β, massive crystals showed similar dependence to the case of TNF-α, while acicular crystals showed nearly the same level for the sizes below and over 10 μm. This suggests that TNF-α and IL-1β represent the different nature of stimulus in inflammation (Watari *et al.* 1997). TNF-α is closely related to phagocytosis, while IL-1β reflects not only the stimulus by phagocytosis but also by particle shape such as acicular form. Even for particles larger than 10 μm, IL-1β is released when cells are stimulated physicomechanically by steeple apexes of needle crystals. This arouses the inflammation reaction cascade and contributes partly to the toxicity of asbestos and other needle shaped particles with a high aspect ratio.

4.7. Characteristics and toxicity of non-specific, physical particle size effect

Physical particle size and shape effect occurs non-specifically in any material and it is irrelevant to the specific surface area effect. The effect appears more clearly and purely in bioactive and bioinert materials, which are minimally affected by chemical dissolution effects. However, the absolute level of stimulation such as IL-1β (figure 7) and TNF-α (figures 9 and 11) by these particles is very low, as small as 1/1000 to 1/10000, compared with endotoxin or lipopeptide (Kiura *et al.* 2005; Watari *et al.* 2007*a*). Therefore, this would not cause serious problems in the short term and in small quantities. However, since it still induces phagocytosis in cells and inflammation in tissue *in vivo*, it leads to chronic inflammation in the case of a large amount and a long-term exposure. The most typical serious cases are osteolysis by abraded particles (Tamura, Y. *et al.* 2002*a*,*b*; Uo *et al.* 2005*b*, 2007; Zhu & Watari 2007) in artificial joint and mesothelioma in asbestos (Watari *et al.* 2006). The lifetime of an artificial joint is sometimes limited to less than 10 years by osteolysis following the inflammation induced by abraded particles. In asbestos, the phagocytosis of acicular particles by alveolar macrophages is insufficiently completed due to their large longitudinal length and non-biodegradability. This results in cell death, cytokine emission and another differentiation of phagocytes. The long-term repetition of this phagocytosis cycle leads to chronic inflammation with superoxide production to attack foreign objects. Superoxides also hurt the DNA of the biological organism itself and cause carcinogenesis when the accumulation of defects in DNA surpasses the certain threshold.

4.8. Competitive effects of composition and particle size

Macroscopic Ni inserted in soft tissue induced necrosis in the nearby periphery (figure 2*a*) and heavy inflammation in the distant region. XSAM analysis revealed that these toxicity levels are due to the concentration of dissolved Ni ions (Uo *et al.* 1999, 2001*a*,*b*, 2006). The strong toxicity of Ni is originated mainly from its dissolved ions. Ni also showed the particle size dependence in cell functional testing, but the values of TNF-α expression (figure 9) were lower than those of Ti and Fe, although Ni has a stronger toxicity. The significantly lower cell survival rate and higher LDH values revealed in the past study indicated that cell destruction occurred with higher probability by exposure to Ni particles as seen in figure 3*a*. The effect of cell death might surpass the stimulatory effect of Ni and suppress the emission of TNF-α.

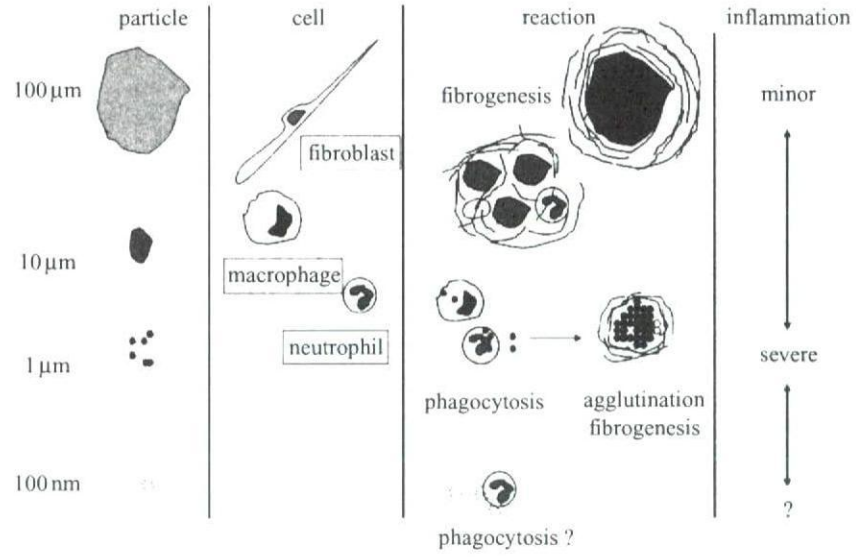

Figure 22. Origin of physical particle size effect: relationship between particle size and cell/tissue (Watari *et al.* 2007*a*).

In reality, most of the materials have some solubility. In those cases, both compositional effect, i.e. toxicity by surface area effect, and physical size effect appear by nanosizing. However, the chemical toxicity by specific surface area effect is far stronger and much more serious and acute, as shown in the case of Ni. Compared to this, the toxicity by physical particle size effect is regarded as nearly negligible (Kiura *et al.* 2005; Watari *et al.* 2007*a*). Therefore, for the soluble materials, both compositional and size effects appear, but size effect is negligible and compositional effect is dominant. For non-soluble or biocompatible materials, chemical ionic dissolution effect is negligible; therefore, pure physical particle size effect appears and becomes prominent.

4.9. Origin of particle size effect: relative size relationship with cells/tissue

The cell and tissue reaction changes from bulk to fine particles for the same material. Figure 22 shows the size relation between particle size and cells/tissues. The cell-stimulative and tissue-inflammatory nature of particles in the micro/nanorange originates from the relative size relationship with the cell/tissue (Watari *et al.* 2007*a*). The reaction inherent to the physical particle effect starts at approximately 100 μm and increases as size decreases. The micro/nanosizing of materials to below cell size makes them 'biointeractive' with cells and tissues (figure 1*b*) and leads to the conversion of functions through biological process as discussed below in §4.11. For less than 200 nm, stimulus diminishes towards the level of macro.

This is clearly distinguished from chemical reactivity enhancement effect by increase in a specific surface area (downwards in figure 1*a*). This originated solely from material properties to enhance greatly the same functions as those in the macroscopic size. Catalyst is a typical example of this effect and no biological interaction is involved.

4.10. Bioactive, biointeractive and bioreactive

Thus, the particles below cell size, approximately 10 μm become, we may say, biointeractive, since that size arouses phagocytosis in cells and inflammation to tissues irrespective of material type, and such a size can be 'biointeractable'. Usually, the term 'bioactive' is used for the nature to induce the intrinsic function of biological organism, in a positive sense to become merit for human beings. The typical example is HAP, which induces osteoconductivity and biocompatibility. However, merit or demerit is just the difference in evaluation system, whether they match the purpose of human beings or unintentionally appear to be against it. Irrespective of that, expression mechanisms stand on the same basis. If we generalize the meaning to the properties to induce the intrinsic function of biological organisms, whether it works as merit or demerit, micro/nano particles can be called bioactive in a more generalized sense. Since it is necessary to distinguish this from the usual use in a positive sense, we may use the word 'bioreactive' instead of bioactive for a more general meaning to induce the intrinsic function. Then we can say that micro/nanoparticles are bioreactive, where the size itself induces the reaction of biological body and may work both positively and negatively.

4.11. Conversion of functions by nanosizing through biological process

We have noted the phenomena of function conversion occurring by nanosizing for certain materials. The examples include the cases of Ti from its biocompatible nature in macroscale to inflammation, leading to osteolysis, in abraded micro/nanoparticles produced from an artificial joint and asbestos from a non-toxic composite of clay minerals (silicate) to carcinogenicity of mesothelioma in the needle-shaped nanoparticles. The mechanism involved in these conversions of function is based on the biological process of particle–cell/tissue interaction (figure 1*b*), originated

from a physical size relationship (figure 22). Whatever materials they may be, nanosizing induces a non-specific reaction and the intrinsic functions of biological organisms. This may lead to the conversion of functions under certain conditions as seen in Ti and asbestos. The bioreaction of cell toxicity and tissue inflammation develops through the conversion of functions to impact on cell proliferation and tissue regeneration. We show further examples in the following.

4.12. Change from non-resorbable to resorbable apatite by nanosizing

Apatite has excellent biocompatibility and induces new bone formation to its surface after implantation in bone circumstances. However, when it becomes micro/nanoparticles, apatite also induces phagocytosis to cells and inflammation to tissue. One of the causes of failures of dental implants is the dust or fine particles of apatite produced by dropout, exfoliation, delamination or abrasion. These induce inflammation in the periphery part of implant, which leads to the resorption of newly formed bone and coated apatite. This sometimes causes failures of dental implant as seen in figure 15. This is a similar type of conversion of functions as the case of abraded Ti particles.

Synthetic HAP exhibits excellent osteoconductivity in a macroscopic size, but it is not substituted for bone and remains permanently in the body. Therefore, it is suitable for use as an implant (Watari *et al.* 1997, 2004). Meanwhile, it is well known that natural bone is composed of collagen and nanoapatite crystallites of approximately 50 nm (Watari 2001, 2005). When the nanocomposites of apatite and collagen fibrils were biomimetically synthesized (Liao *et al.* 2005, 2007*a–c*; Gelinsky *et al.* 2007; Li *et al.* 2008*a*,*d*) and implanted in subcutaneous tissue, they were covered with fibrous connective tissue and then mostly resorbed in eight weeks by phagocytosis (Yokoyama *et al.* 2005*b*). Therefore, nanoapatite composites are bioresorbable.

When they were implanted in hard tissue situations such as bone defects or bone marrow, inflammation was induced, and osteoclasts and osteoblasts were then differentiated. Phagocytosis of nanoapatite composites by osteoclasts and osteogenesis by osteoblasts occurred simultaneously and adjacently to each other, as shown in figure 16. This tendency progressed with time and nanoapatite composites were finally replaced with new bone. The phenomena of resorption and bone formation were similar to the case of autologous bone graft. This process is also similar to the remodelling process of natural bone occurring constantly in our body (Yokoyama *et al.* 2005*b*). As a result, nanoapatite composites work as bone-substitute materials for hard-tissue reconstruction. Thus, nanosizing leads to another type of conversion of function from an osteoconductive, but non-bone substitutional nature in macro to bone substitutional properties in nano through a biologically induced process (Watari *et al.* 2008*c*).

4.13. Change from non-cell-adhesive graphite to cell adhesive CNT

Graphite and CNTs are isomorphs of carbon and composed of a similar graphene sheet in crystal structure. As an element, carbon (C) would be bioinert. However, graphite and CNTs show a contrasting difference in cell attachment (figures 17 and 18) and proliferation (figure 19), being very low for graphite and excellent for CNTs. CNTs adhere to collagen fibrils, a kind of protein, exposed on dentin surface by acid etching (Akasaka *et al.* in press *b*). This affinity of CNTs to proteins and also saccharides (Akasaka & Watari 2008) leads to the high adsorption of proteins (figure 20), including growth factors contained in the FBS added in the cell culture medium. This improves compatibility on the surface of CNTs, which is the basis for excellent cell adhesion (Akasaka *et al.* in press *a*), growth and functional expression of ALP activity (figure 20), a marker of osteogenesis capability (Aoki *et al.* 2007*a*; Li *et al.* 2008*b*,*c*). It is to be added that the precipitation of nanoapatite or calcium phosphate with a low crystallinity occurring in the simulated body fluid (SBF) also contributes to the improvement of biocompatibility (Akasaka & Watari 2005; Akasaka *et al.* 2005).

There are several factors that contribute to the affinity of CNTs to proteins. They include the similarity in composition, similarity in crystal structure, nano-network architecture in morphology, surface area, surface electronic charge and hydrophobic/hydrophilic properties. The hydrophobic interaction between carbon and proteins is generally counted for protein adsorption, but this could not explain the contrasting difference between graphite and CNTs, isomorphs of carbon, shown in figure 20.

The specific sites of adsorption of biological proteins in serum or tissue fluid are another matter of interest (Lundqvist *et al.* 2008). They are produced especially if CNTs are treated with acid or modified with some receptors. They provide more chemical and direct atomic binding between CNTs and proteins, which is important to create specific binding to particular targets. The existence of such sites is suggested from an experimental observation that the nucleation of acicular nanoapatite crystallites in SBF with added fluorine ions occurs radially from certain sites on CNTs (Akasaka *et al.* 2005). Although the contribution of specific sites is important, CNTs adsorb proteins even without such sites. The adsorption shown in this paper (figure 20) is mostly due to the more general, non-specific, physical adsorption. The nanometric curvature of graphene sheets composed of sixfold carbon rings in the tube atomic structure of CNTs generates a strong tendency to agglomerate by themselves and also an affinity to similar structures, one of which is protein.

Another factor that provides cell-adhesive properties is related to their structure. Although CNTs generally have a tendency to agglomerate and form bundles, the wavy and fibrous agglomeration still makes a nano-meshwork conformation with a large porosity where cells can take nutrient elements or growth factors easily.

In addition to this, the nanosize diameter of CNT fibres, a few to several tens of nm, is close to that of filopodia of cells, approximately 100 nm as seen in figure 18*b*, which provides easy conditions for the filopodia to interact with a CNT network. Trypsin is generally used for the detachment of cells from a scaffold. On a CNT scaffold, however, cells cannot separate well because of the strong binding of filopodia, which is sometimes mechanical binding, with a CNT network. It demonstrates the good cell adhesivity of CNTs (Aoki *et al.* 2005). Bacteria of submicron to micrometre size are also trapped by the fine, wavy nanodiameter of a SWCNT string in the manner of winding around them (Akasaka & Watari 2009). These are another example that micro/nano-sized materials become biointeractable with biological objects of comparable size, in these cases with filopodia and bacteria. The Nano-meshwork structure of CNT agglomeration contributes physically to favoured conditions for cell attachment.

4.14. Invasion and internal diffusion of nanoparticles

Stimulus, represented by an amount of TNF-α release in figure 11, which is pronounced below 10 µm, exhibited the maximum from around µm down to 500 nm. For smaller sizes below 200 nm, more typically less than 50 nm, stimulus decreased to nearly the level of macroscopic size (Watari *et al.* 2007*a*). This looks preferable from the point of view of biological application of nanoparticles, since toxicity is apparently decreased. However, this, in turn, means that the biophylactic system does not work well any more against nanoparticles. The invasion of nanoparticles into the body can occur for this range of particle size. Nanoparticles might be the objects whose existence has not been assumed in the body defence system of a living organism.

It is known that particles below 10 µm can pass through the bronchial. For further smaller ones, they may reach lung pulmonary alveoli where they are taken up directly into blood vessels. Thus, they can invade into the internal body through the respiratory system (figure 12) and also through the digestive system at the intestinal wall (figure 13). Then they diffuse through the cardiovascular system for the whole body from organ to organ (figure 14). The behaviour of internal diffusion is different, depending on materials, for example, TiO_2 and Pt (Watari *et al.* 2007*c*,*d*, 2008*a*, 2009; Abe *et al.* 2009, in press *a*,*b*,*c*).

4.15. Non-specificity of particle-inducing bioreaction

There are many pathways for living organisms to recognize foreign objects. Macrophages discriminate biohazardous objects such as bacteria and make an initial response specific to each object. The absolute intensity of TNF-α expression against endotoxin or lipopeptide is far higher than physical size effect. Toxicity by bacteria or rejection response caused by certain proteins is much stronger. One of the recognition paths is through the toll-like receptor (TLR). In some cases, they discriminate by different sugar chain patterns. In this way, both innate and acquired immune systems work against micro-organisms and proteins, mostly in specific manner.

On the other hand, in the case of materials, the present *in vitro* and *in vivo* experiments showed that (i) a similar particle size dependence of expression of superoxide and cytokines irrespective of the different nature of materials with bioinert or bioactive properties (figure 9).

These indicate that (ii) the reaction is non-specific and any particles below cell size are regarded as foreign objects by cells including neutrophils and macrophages, which induces phagocytosis whatever the material as observed *in vitro* (figure 3) and *in vivo* (figures 4 and 10).

(iii) Toxicity level shown as an absolute intensity of superoxide production, cytokines IL-1β and TNF-α expression by micro/nanoparticles is very low compared with endotoxin (Kiura *et al.* 2005; Watari *et al.* 2007*a*).

(iv) TLR is not sensitive and rather inert to particles of materials according to our different studies.

There is always a serious rejection reaction for organ transplantation from one person to another, where the difference in individuals is discriminated in a specific identification manner. (v) For the case of materials such as in an implant, there is no strong rejection and it is commonly and generally, therefore, acceptable to any person.

All these demonstrate that the acquired immune systems do not work and only some of the innate immune systems are activated against materials. Non-actuation of immune systems, except a few innate immunity processes and lack of other recognition paths to materials, limits the recognition routes and reactions to fewer possibilities. One of the most frequently encountered actuations is a phagocytosis reaction with the dependency only on particle size, and another is stimulus, sometimes mechanical, by particle shape when a pointing needle form. This lack of recognition paths shows the characteristics of an non-specific nature to particle bioreaction, occurring irrespective of materials. The lack of recognition paths is also one of the central reasons that the body defence system cannot respond well to nanoparticles, and (vi) they can invade directly into the internal body through the respiratory and digestive system, rather easily and non-specifically.

These numbered facts (i)–(vi) in the above symbolize the non-specificity in the characteristics of nanoparticles in relation to biological organisms.

4.16. Biointeractable critical size: relationships with cells and viruses

The critical sizes where the transition of material behaviour against biological organisms occurs are at approximately 100 µm, 10 µm and 200 nm. Materials start to behave with the characteristics of particles from approximately 100 µm and below. In the case of a needle shape, this critical value would be larger to some extent. The critical sizes, 10 µm to become biointeractable

through the induction of phagocytosis in cells and inflammation to tissues and 200 nm, most typically less than 50 nm, to be less stimulative and become able to invade into the body, are approximately coincident with the average size of cells and viruses, respectively.

Is there any reason for these critical sizes to be the level of cell and virus? This coincidence may not be by accident.

When the particle size becomes nearly the same as cell size, approximately 10 μm or smaller, the object becomes biointeractive. Macrophages discriminate objects and initiate specific reactions, which are followed by the activation of T lymphocytes and others against bacteria and virus. In the case of materials, most such immune systems and recognition paths do not work and only the process that senses the particle size remains, regarding non-specifically the objects smaller than cells as foreign objects. This induces phagocytosis, followed by the formation of lysosome in cells and treatment in it.

The lack of recognition paths in the immune system makes objects of a size similar to viruses less stimulative. The insufficient immunity makes them able to invade the internal body and cells through the pulmonary alveolus, intestine or other paths as viruses can enter. This is in contrast to the case of a virus where the specific immune system is actuated and invasion may be blocked. Thus, the object size permissible to invade becomes the level of virus.

4.17. Antagonism of nanotechnology and nanotoxicology

The recognition of physical particle size and shape effect is the essential basis for the proper understanding of the nanosizing effect and for the development of biomedical applications of nanotechnology. High function and risk assessment often produces antagonism of nanotechnology and nanotoxicology between nanotech-developing researchers and toxicologists. From the viewpoint of bioreactivity of the nanosizing effect as revealed in the present study, they are different sides of an evaluation system for human beings, merit if they match the purpose of human beings or demerit if they unintentionally appear against. However, both originate from the same mechanism. It is necessary to recognize the bilateral nature of nanomaterials, high function and risk, for the proper acknowledgement of the influence on biological organisms and environments and for the development and application of nanotechnology.

5. CONCLUSIONS

The increase in specific surface area usually counted as the nanosizing effect causes the enhancement of chemical reactivity and serious toxicity for soluble and stimulative materials. This is the contribution of compositional effects, and is easily recognized. This effect originates solely from material properties and greatly enhances the same functions as those of a macroscopic size. Catalysts are a typical example of this effect and no biological interaction is involved.

Non-soluble, biocompatible materials show different particle size dependence. The transition of bioreaction occurs at the critical sizes of approximately 100 μm, 10 μm and 200 nm. This physical size effect is non-specific, which is independent of material type, and especially pronounced for a cell size of less than approximately 10 μm. It causes stimulus through the biological process of phagocytosis in cell and inflammation in tissue. When the particle size is 200 nm or less, they become less stimulative and the recognition by body defence systems becomes weaker. They may invade directly into the internal body through the respiratory or digestive system and diffuse inside the whole body.

Thus, the physical micro/nanosizing of materials makes them biointeractive with cells and tissue. These biointeractable particles induce the intrinsic functions and reactions of biological organisms. They become bioreactive and may work both in merit and demerit ways. The bioreactive nature causes inflammation, and this leads to the occurrence of conversion of functions of materials through biological processes such as from biocompatibility to stimulus in Ti-abraded particles and asbestos, from non-bone substitutional to bone substitutional in nanoapatite and from non-cell adhesive to cell adhesive CNTs.

This effect has its origin in the biological interaction process between particles and cells/tissue. Non-actuation of immune system, except for a few innate immunity processes and limitation of recognition paths for materials, gives the non-specific nature to particle bioreaction and restricts the recognition routes to the size-sensitive phagocytosis reaction. This insensitive nature also permits nanoparticles below 200 nm to slip through the body's defence system and invade directly into the internal body.

The characteristic phenomena of no rejection reactions to artificial organs in macro, non-specific phagocytosis to cells and inflammation to tissue in micro and direct invasion into the internal body in nano originate on the same basis that the actuation of immune system is limited to the few possibilities of innate immunity for materials.

The acknowledgement of the physical particle size effect and the bilateral nature of nanomaterials with possibilities of high functions and risks is the essential basis for the proper understanding of the nanosizing effect and for the development of biomedical applications of nanotechnology.

Animal experiments were performed in accordance with the Guide for the Care and Use of Laboratory Animals, Hokkaido University Graduate School of Dental Medicine.

The present study was performed under the support of Health and Labour Sciences Research Grants in Research on Chemical Substance Assessment from the Ministry of Health, Labour and Welfare of Japan (H18-Chemistry-General-006).

REFERENCES

Abe, S., Koyama, C., Akasaka, T., Uo, M., Kuboki, K. & Watari, F. 2009 Internal distribution of several inorganic microparticles in mice. *Bioceramics* **21**, 539–542. (Key engineering materials, vols. 396–398; *Trans. Tech. Publications*)

Abe, S. *et al.* In press *a*. Biodistribution imaging of magnetic nanoparticles in mice compared with X-ray scanning analytical microscopy and magnetic resonance imaging. *Bio-Med. Mater. Eng.*

Abe, S., Koyama, C., Esaki, M., Akasaka, T., Uo, M., Kuboki, K., Morita, M. & Watari, F. In press *b*. *In vivo* internal diffusion of several inorganic microparticles through an oral administration. *Bio-Med. Mater. Eng.*

Abe, S., Koyama, C., Uo, M., Akasaka, T., Kuboki, K. & Watari, F. In press *c*. Time-dependence and visualization of TiO_2 and Pt particle biodistribution in mice. *J. Nanosci. Nanotechnol.*

Akasaka, T. & Watari, F. 2005 Nano-architechture on carbon nanotube surface by biomimetic coating. *Chem. Lett.* **34**, 826–827. (doi:10.1246/cl.2005.826)

Akasaka, T. & Watari, F. 2008 Carbohydrate coating of carbon nanotubes for biological recognition. *Fullerenes Nanotubes Carbon Nanostruct.* **16**, 114–125. (doi:10.1080/15363830801887992)

Akasaka, T. & Watari, F. 2009 Capture of bacteria by flexible carbon nanotubes. *Acta Biomater.* **5**, 607–612. (doi:10.1016/j.actbio.2008.08.014)

Akasaka, T., Watari, F., Sato, Y. & Tohji, K. 2005 Apatite formation on carbon nanotubes. *Mater. Sci. Eng. C* **26**, 675–678. (doi:10.1016/j.msec.2005.03.009)

Akasaka, T., Yokoyama, A., Matsuoka, M., Hashimoto, T., Abe, S., Uo, M. & Watari, W. In press *a*. Adhesion of human osteoblast-like cells (Saos-2) to carbon nanotube sheets. *Bio-Med. Mater. Eng.*

Akasaka, T., Nakata, K., Uo, M. & Watari, F. In press *b*. Modification of the dentin surface by using carbon nanotubes. *Bio-Med. Mater. Eng.*

Aoki, N., Yokoyama, A., Nodasaka, Y., Akasaka, T., Uo, M., Sato, Y., Tohji, K. & Watari, F. 2005 Cell culture on a carbon nanotube scaffold. *J. Biomed. Nanotechnol.* **1**, 402–405. (doi:10.1166/jbn.2005.048)

Aoki, N., Yokoyama, A., Nodasaka, Y., Akasaka, T., Uo, M., Sato, Y., Tohji, K. & Watari, F. 2006 Strikingly extended morphology of cells grown on carbon nanotubes. *Chem. Lett.* **35**, 508–509. (doi:10.1246/cl.2006.508)

Aoki, N., Akasaka, T., Watari, F. & Yokoyama, A. 2007*a* Carbon nanotubes as scaffolds for cell and effect on cellular functions. *Dent. Mater. J.* **26**, 178–185. (doi:10.4012/dmj.26.178)

Aoki, N., Yokoyama, A., Nodasaka, Y., Akasaka, T., Uo, M., Sato, Y., Tohji, K. & Watari, F. 2007*b* Carbon nanotubes deposited on titanium implant for osteoblast attachment. *J. Bionanosci.* **1**, 14–16. (doi:10.1166/jbns.2007.003)

Asakura, K., Chun, W. J., Tohji, K., Sato, Y. & Watari, F. 2005 X-ray absorption fine structure studies on the local structures of Ni impurities in a carbon nanotube. *Chem. Lett.* **34**, 382–383. (doi:10.1246/cl.2005.382)

Chan, W. C. W., Maxwell, D. J., Gao, X., Bailey, R. E., Han, M. & Nie, S. 2002 Luminescent quantum dots for multiplexed biological detection and imaging. *Curr. Opin. Biotechnol.* **13**, 40–46. (doi:10.1016/S0958-1669(02)00282-3)

Fugetsu, B. *et al.* 2004*a* Caged multi-walled carbon nanotubes as the adsorbents for affinity-based elimination of ionic dyes. *Environ. Sci. Technol.* **38**, 6890–6896. (doi:10.1021/es049554i)

Fugetsu, B., Satoh, S., Iles, A., Tanaka, K., Nishi, N. & Watari, F. 2004*b* Encapsulation of multi-walled carbon nanotubes (MWCNTs) in Ba^{2+}-alginate toform coated micro-beads and their application to the pre-concentration/elimination of dibenzo-p-dioxin, dibenzofuran, and biphenyl from contaminated water. *Analyst (London)* **129**, 565–566. (doi:10.1039/b405325g)

Gelinsky, M. *et al.* 2007 Biomaterials based on mineralised collagen an artificial extracellular bone matrix. In *Interface oral health science 2007* (eds M. Watanabe & O. Okuno), pp. 323–328. Tokyo, Japan: Springer.

Kiura, K., Sato, Y., Yasuda, M., Fugetsu, B., Watari, F., Tohji, K. & Shibata, K. 2005 Activation of human monocytes and mouse splenocytes by single-walled carbon nanotubes. *J. Biomed. Nanotechnol.* **1**, 359–364. (doi:10.1166/jbn.2005.031)

Kumazawa, R., Watari, F., Takashi, N., Tanimura, Y., Uo, M. & Totsuka, Y. 2002 Effects of Ti ions and particles on cellular function and morphology of neutrophils. *Biomaterials* **23**, 3757–3764. (doi:10.1016/S0142-9612(02)00115-1)

Li, X. M., Van Blitterswijk, C. A., Feng, Q. L., Cui, F. Z. & Watari, F. 2008*a* The effect of calcium phosphate microstructure on bone-related cells *in vitro*. *Biomaterials* **29**, 3306–3316. (doi:10.1016/j.biomaterials.2008.04.039)

Li, X. M., Gao, H., Uo, M., Sato, Y., Akasaka, T., Feng, Q. L., Cui, F. Z., Lui, M. H. & Watari, F. 2008*b* Effect of carbon nanotubes on cellular functions *in vitro*. *J. Biomed. Mater. Res. A.* (doi:10.1002/jbm.a.32203)

Li, X. M. *et al.* 2008*c* Maturation of osteoblast-like SaoS2 induced by carbon nanotubes. *Biomed. Mater.* **4**, 015 005. (doi:10.1088/1748-6041/4/1/015005)

Li, X. M., Lui, X. H., Dong, W., Feng, Q. L., Cui, F. Z., Uo, M., Akasaka, T. & Watari, F. 2008*d* *In vitro* evaluation of porous poly(L-lactic acid) scaffold reinforced by chitin fibers. *J. Biomed. Mater. Res. B.* (doi:10.1002/jbm.b.31311)

Liao, S., Wang, W., Uo, M., Ohkawa, S., Akasaka, T., Tamura, K., Cui, F. & Watari, F. 2005 A three-layered nano-carbonated hydroxyapatite/collagen/PLGA composite membrane for guided tissue regeneration. *Biomaterials* **26**, 7564–7571. (doi:10.1016/j.biomaterials.2005.05.050)

Liao, S., Watari, F., Zhu, Y., Uo, M., Akasaka, T., Wang, W., Xu, G. & Cui, F. 2007*a* The degradation of the three layered nano-carbonated hydroxyapatite/collagen/PLGA composite membrane *in vitro*. *Dent. Mater.* **23**, 1120–1128. (doi:10.1016/j.dental.2006.06.045)

Liao, S., Watari, F., Xu, G., Ngiam, M., Ramakrishna, S. & Chan, C. K. 2007*b* Morphological effects of variant carbonates in biomimetic hydroxyapatite. *Mater. Lett.* **61**, 3624–3628. (doi:10.1016/j.matlet.2006.12.007)

Liao, S., Ngiam, M., Watari, F., Ramakrishna, S. & Chan, C. K. 2007*c* Systematic fabrication of nano-carbonated hydroxyapatite collagen composites for biomimetic bone grafts. *Bioinspir. Biomim.* **2**, 37–41. (doi:10.1088/1748-3182/2/3/001)

Liao, S., Xu, G., Wang, W., Watari, F., Cui, F., Ramakrishna, S. & Chan, C. K. 2007*d* Self-assembly of nano-hydroxyapatite on multi-walled, carbon nanotubes. *Acta Biomater.* **3**, 669–675. (doi:10.1016/j.actbio.2007.03.007)

Lundqvist, M., Stigler, J., Elia, G., Lynch, I., Cedervall, T. & Dawson, K. A. 2008 Nanoparticle size and surface properties determine the protein corona with possible implications for biological impacts. *Proc. Natl Acad. Sci. USA* **105**, 14 265–14 270. (doi:10.1073/pnas.0805135105)

Matsuno, H., Yokoyama, A., Watari, F., Uo, M. & Kawasaki, T. 2001 Biocompatibility and osteogenesis of refractory metal implants, titanium, hafnium, niobium, tantalum and rhenium. *Biomaterials* **22**, 1253–1262. (doi:10.1016/S0142-9612(00)00275-1)

Matsuo, S., Watari, F. & Ohata, N. 2001 Fabrication of functionally graded dental composite resin post and core

by laser lithography and finite element analysis of its stress relaxation effect on tooth root. *Dent. Mater. J.* **20**, 257–274.

Moller, W., Felten, K., Kohlhaufl, M., Haussinger, K. & Kreyling, W. G. 2007 Motion and twisting of magnetic particles ingested by alveolar macrophages in non-smokers and smokers: implementation of viscoelasticity. *J. Magn. Magn. Mater.* **311**, 269–274. (doi:10.1016/j.jmmm.2006.10.1177)

Moller, W., Meyer, G. & Kreyling, W. G. 2008 Advances in lung imaging techniques for the treatment of respiratory disease. *Drug Discov. Today Ther. Strateg.* **5**, 87–92. (doi:10.1016/j.ddstr.2008.06.002)

Rosca, I. D., Watari, F. & Uo, M. 2004 Microparticle formation and its mechanism in single and double emulsion solvent evaporation. *J. Control. Rel.* **99**, 271–280. (doi:10.1016/j.jconrel.2004.07.007)

Rosca, I. D., Watari, F., Uo, M. & Akasaka, T. 2005 Oxidation of multiwalled carbon nanotubes by nitric acid. *Carbon* **43**, 3124–3131. (doi:10.1016/j.carbon.2005.06.019)

Sato, Y. *et al.* 2005*a* Strict preparation and evaluation of water-soluble hat-stacked carbon nanofibers for biomedical application and their high biocompatibility: influence of nanofiber-surface functional groups on cytotoxicity. *Mol. BioSyst.* **1**, 142–145. (doi:10.1039/b501222h)

Sato, Y. *et al.* 2005*b* Influence of length on cytotoxicity of multi-walled carbon nanotubes against human acute monocytic leukemia cell line THP-1 *in vitro* and subcutaneous tissue of rats *in vivo*. *Mol. BioSyst.* **1**, 176–182. (doi:10.1039/b502429c)

Smith, A. M., Duan, H., Mohs, A. M. & Nie, S. 2008 Bioconjugated quantum dots for *in vivo* molecular and cellular imaging. *Adv. Drug Deliv. Rev.* **60**, 1226–1240. (doi:10.1016/j.addr.2008.03.015)

Takagi, A., Hirose, A., Nishimura, T., Fukumori, N., Ogata, A., Ohashi, N. & Kanno, J. 2008 Induction of mesothelioma in p53 + / − mouse by intraperitoneal application of multi-wall carbon nanotube. *J. Toxic. Sci.* **33**, 105–116. (doi:10.2131/jts.33.105)

Tamura, K., Takashi, N., Kumazawa, R., Watari, F. & Totsuka, Y. 2002 Effects of particle size on cell function and morphology in titanium and nickel. *Mater. Trans.* **43**, 3052–3057. (doi:10.2320/matertrans.43.3052)

Tamura, Y., Yokoyama, A., Watari, F., Uo, M. & Kawasaki, T. 2002*a* Mechanicalproperties of surface-nitrided titanium for abrasion resistant implant materials. *Mater. Trans.* **43**, 3043–3051. (doi:10.2320/matertrans.43.3043)

Tamura, Y., Yokoyama, A., Watari, F. & Kawasaki, T. 2002*b* Surface properties and biocompatibility of nitrided titanium for abrasion resistant implant materials. *Dent. Mater. J.* **21**, 355–372.

Uo, M., Watari, F., Yokoyama, A., Matsuno, H. & Kawasaki, T. 1999 Dissolution of nickel and tissue response observed by X-ray analytical microscopy. *Biomaterials* **20**, 747–755. (doi:10.1016/S0142-9612(98)00224-5)

Uo, M., Watari, F., Yokoyama, A., Matsuno, H. & Kawasaki, T. 2001*a* Tissue reaction around metal implants observed by X-ray scanning analytical microscopy. *Biomaterials* **21**, 677–685. (doi:10.1016/S0142-9612(00)00230-1)

Uo, M., Watari, F., Yokoyama, A., Matsuno, H. & Kawasaki, T. 2001*b* Visualization and detectability of rarely contained elements in soft tissue by X-ray scanning analytical microscopy and electron probe micro analysis. *Biomaterials* **22**, 1787–1794. (doi:10.1016/S0142-9612(00)00349-5)

Uo, M., Tamura, K., Sato, Y., Yokoyama, A., Watari, F., Totsuka, Y. & Tohji, K. 2005*a* The cytotoxicity of metal-encapsulating carbon nanocapsules. *Small* **1**, 816–819. (doi:10.1002/smll.200400143)

Uo, M., Asakura, K., Yokoyama, A., Tamura, K., Totsuka, Y., Akasaka, T. & Watari, F. 2005*b* Analysis of titanium dental implants surrounding soft tissue using X-ray absorption fine structure (XAFS) analysis. *Chem. Lett.* **34**, 776–777. (doi:10.1246/cl.2005.776)

Uo, M., Asakura, K., Kohgo, T. & Watari, F. 2006 Selenium distribution in human soft tissue determined by using X-ray scanning analytical microscope and X-ray absorption fine structure analysis. *Chem. Lett.* **35**, 66–67. (doi:10.1246/cl.2006.66)

Uo, M., Asakura, K., Yokoyama, A., Ishikawa, M., Tamura, K., Totsuka, Y., Akasaka, T. & Watari, F. 2007 X-ray absorption fine structure (XAFS) analysis of titanium-implanted soft tissue. *Dent. Mater. J.* **26**, 268–273. (doi:10.4012/dmj.26.268)

Ushiro, M., Uno, K., Fujikawa, T., Sato, Y., Tohji, K., Watari, F., Chun, W., Koike, Y. & Asakura, K. 2006 X-ray absorption fine structure (XAFS) analyses of Ni species trapped in graphene sheet of carbon nanofibers. *Phys. Rev. B* **73**, 144103-1–144103-11. (doi:10.1103/PhysRevB.73.144103)

Wang, W., Omori, M., Watari, F. & Yokoyama, A. 2005 Novel bulk carbon materials for implant by spark plasma sintering. *Dent. Mater. J.* **24**, 478–486.

Wang, W., Watari, F., Omori, M., Liao, S., Yokoyama, A., Uo, M. & Ohkubo, A. 2007 Mechanical properties and biological behavior of carbon nanotube/polycarbosilane composites for implant materials. *J. Biomed. Mater. Res. B Appl. Biomater.* **82b**, 223–230. (doi:10.1002/jbm.b.30724)

Watari, F. 2001 Compositional and morphological imaging of laser irradiated human teeth by low vacuum SEM, confocal laser scanning microscopy and atomic force microscopy. *J. Mater. Sci. Med.* **12**, 189–194. (doi:10.1023/A:1008913828931)

Watari, F. 2005 *In situ* quantitative analysis of etching process of human teeth by atomic force microscopy. *J. Electron Microsc.* **54**, 299–308. (doi:10.1093/jmicro/dfi056)

Watari, F., Yokoyama, A., Saso, F., Uo, M. & Kawasaki, T. 1997 Fabrication and properties of functionally graded dental implant. *Composites B* **28**, 5–11. (doi:10.1016/S1359-8368(96)00021-2)

Watari, F., Yokoyama, A., Omori, M., Hirai, T., Kondo, H., Uo, M. & Kawasaki, T. 2004 Biocompatibility of materials and development to functionally graded implant for bio-medical application. *Compos. Sci. Technol.* **64**, 893–908. (doi:10.1016/j.compscitech.2003.09.005)

Watari, F., Inoue, M., Akasaka, T., Sakaguchi, N., Ichinose, H. & Uo, M. 2006 Comparison of morphology and behavior of carbon nanotubes and asbestos. In *Proc. 6th Asian BioCeramics Symp.*, pp. 142–145.

Watari, F. *et al.* 2007*a* Biochemical and pathological responses of cells and tissue to micro- and nanoparticles from titanium and other materials. In *Handbook of biomineralization*, vol. 3 (ed. E. Bauerlein), pp. 127–144. Weinheim, Germany: Wiley-VCH.

Watari, F. *et al.* 2007*b* Effect of nanosizing of materials on living organism. In *Proc. Int. Symp. Nano Science and Technology (ISNST) 2007*, pp. 43–52. Tainan, Taiwan: Southern Taiwan University.

Watari, F. *et al.* 2007*c* Internal motion of micro/nano particles of titanium oxides and others in the body. *Archiv. BioCeramics Res.* **7**, 13–18. (*Proc. Asian BioCeramics Symposium* 2007.)

Watari, F., Abe, S., Tamura, K., Uo, M., Yokoyama, A. & Totsuka, Y. 2007*d* Internal diffusion of micro/nanoparticles inside body. *Bioceramics* **20**, 95–98. (Key engineering materials, vols. 361–363; *Trans. Tech. Publications*).

Watari, F. *et al.* 2008*a* Behavior of *in vitro*, *in vivo* and internal motion of micro/nano particles of titanium, titanium oxides and others. *J. Ceram. Soc. Jpn* **116**, 1–5. (doi:10.2109/jcersj2.116.1)

Watari, F., Inoue, S., Takashi, N., Totsuka, Y. & Yokoyama, A. 2008*b* Reaction of cells and tissue to material nanosizing. *Trans. Mater. Res. Soc. Jpn.* **33**, 209–214.

Watari, F., Yokoyama, A., Gelinsky, M. & Pompe, W. 2008*c* Conversion of functions by nanosizing—from osteoconductivity to bone substitutional properties in apatite. In *Interface oral health science 2007* (eds M. Watanabe & O. Okuno), pp. 139–147. Japan, Tokyo: Springer.

Watari, F. *et al.* 2009 Visualization of invasion into the body and internal diffusion of nanoparticles. *Bioceramics* **21**, 569–572. (Key engineering materials, vols. 396–398; *Trans. Tech. Publications.*)

Yokoyama, A. *et al.* 2005*a* Biological behavior of hat-stacked carbon nanofibers in the subcutaneous tissue in rats. *Nano Lett.* **5**, 157–161. (doi:10.1021/nl0484752)

Yokoyama, A., Gelinsky, M., Kawasaki, T., Kohgo, T., Konig, U., Pompe, W. & Watari, F. 2005*b* Biomimetic porous scaffolds with high elasticity made from mineralized collagen—an animal study. *J. Biomed. Mater. Res. Appl. Biomater.* **75b**, 464–472. (doi:10.1002/jbm.b.30331)

Zhu, Y. & Watari, F. 2007 Surface carbonization of titanium for abrasion-resistant implant materials. *Dent. Mater. J.* **26**, 245–253. (doi:10.4012/dmj.26.245)

JOURNAL of the ROYAL SOCIETY Interface

JOURNAL of the ROYAL SOCIETY Interface

Interface Oral Health Science 2007: 139–148

Conversion of functions by nanosizing—from osteoconductivity to bone substitutional properties in apatite

Fumio Watari[1]*, Atsuro Yokoyama[1], Michael Gelinsky[2], Wolfgang Pompe[2]
[1]*Graduate School of Dental Medicine, Hokkaido University, Sapporo 060-8586, Japan;*
[2]*Max Bergmann Center of Biomaterials, Institute of Materials Science, Technical University, 01069 Dresden, Germany*
*watari@den.hokudai.ac.jp

Abstract. Synthetic hydroxyapatite, in the usual case, of a macroscopic size, exhibits excellent osteoconductivity. However, it is not substituted with natural bone and remains permanently in the body; therefore it is suitable for using as an implant. It is well known that natural bone is composed of collagen and nanocrystallites of apatite with the size of approximately 50 nm. When the composite with collagen and nanoapatite synthesized in the biomimetic aspects is implanted, phagocytosis and inflammation are induced. Osteoclasts and osteoblasts are then differentiated and activated. The bone resemblant material and its phagocytizable nanometer size provide the conditions that composite is biologically degradable through phagocytosis by osteoclasts, and new bone formation by osteoblasts is simultaneously activated and proceeded. As a result, nanocomposite leads to the bone substitutional properties. Thus the conversion of functions is attained for apatite by nanosizing—from osteoconductivity in macroscopic size to bone substitutional properties in nano/micro scale. This tendency is more enhanced for carbonated hydroxyapatite. The mineralization surrounding collagen fibrils determines the crystallization of apatite for their size and orientations. Nanoparticles cause the reaction of cells/tissue and stimulate the occurrence of inflammation, which works as a stimulus in most cases or pronounces the conversion of functions leading to the bioactive properties for some cases, depending on the situation. Nano structure is essential for these stages to be processed.

Key words. nanosizing, apatite, tissue regeneration, inflammation, nanotoxicology

Introduction: non-resorbable and resorbable apatite

Synthetic hydroxyapatite in the usual case, that is, in a macroscopic size, exhibits excellent osteoconductivity. However, it is not substituted for natural bone and remains permanently in the body; therefore it is suitable for using as an implant.

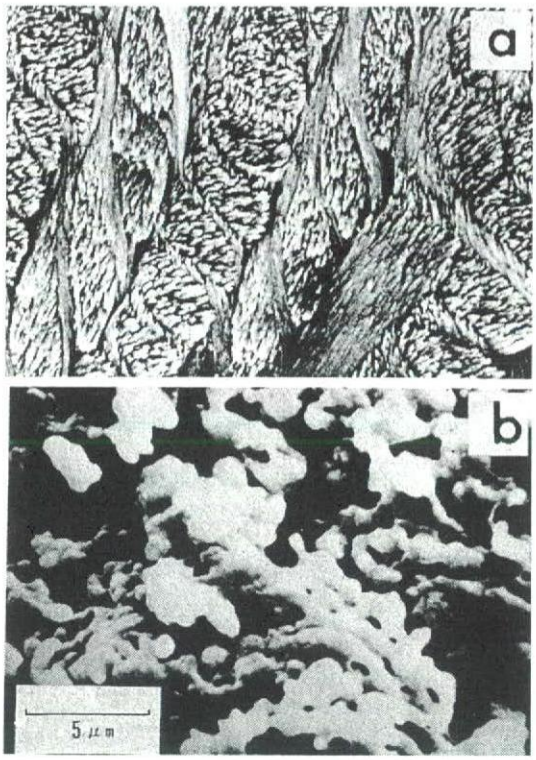

Fig. 1. Difference of morphology of hydroxyapatite. **a** Enamel of molar of rat, **b** sintered synthetic apatite

It is well known that natural bone is composed of collagen and nanocrystallites of apatite with the size of approximately 50 nm. In Fig. 1 the SEM photographs compare the difference in morphology of hydroxyapatite for natural hard tissue, in this case, enamel of molar of rat (a) and sintered synthetic apatite (b). In synthetic apatite the size of particles is a few microns, and they agglomerate in random, while in enamel, enamel prism of about 5 μm is composed of a bunch of apatite crystallites of about 50 nm. It is known that apatite crystallites are grown in their *c*-axis along collagen fibrils. Thus natural hard tissue is regarded as a kind of composite with the preferably oriented structure of nanocrystallites.

There is the difference in behavior between synthetic apatite and bone. Bone is continuously remodeled by resorption and new bone formation. Thus there exist apatites with different behaviors, non-resorbable and resorbable apatites. The problem arises: what is their difference and its cause? We will first see the nanosizing effect in general, and then the case of apatite and its mechanism.

Materials and methods

Both biochemical cell functional tests and animal implantation tests were done to investigate the reaction to fine particles of 99.9% pure Ti, Fe, Ni, and TiO_2 for the various sizes from 300 nm to 150 μm [1]. Human neutrophils were used as probe

cells for various cell toxicity tests, after mixed with particles in Hank's balanced salt solution (HBSS) at 37°C. Histological investigations were done after implanting in the subcutaneous connective tissue of rats.

Hydroxyapatite-collagen composites were synthesized biomimetically on mineralized collagen type I. They have the three-dimensional scaffold structures with the interconnecting pores. They were implanted into the subcutaneous tissue, and bone defects made in the femur of rats for 1–12 weeks and observed histopathologically [2].

Results

Micro/nanosizing effect onto cell/tissue reaction

Figure 2 shows the dependence of TNF-α release from human neutrophils on the size of Ti particles. TNF-α was increased with the decrease in particle size. The increase was pronounced for 0.5 and 3 μm. The release of LDH, superoxide and cytokine Il-1β showed the similar behavior as TNF-α, while cell survival rate showed the inverse decreasing tendency. Under these conditions ICP elemental analysis indicated that the dissolution from Ti particles was negligible below detection limit [1].

Figure 3 shows the SEM image of human neutrophils of control (a) and the one exposed to 0.5 μm Ti particles (b) where a neutrophil extends its pseudopod to phagocytize Ti particles for the size less than 10 μm [3]. For the particles larger

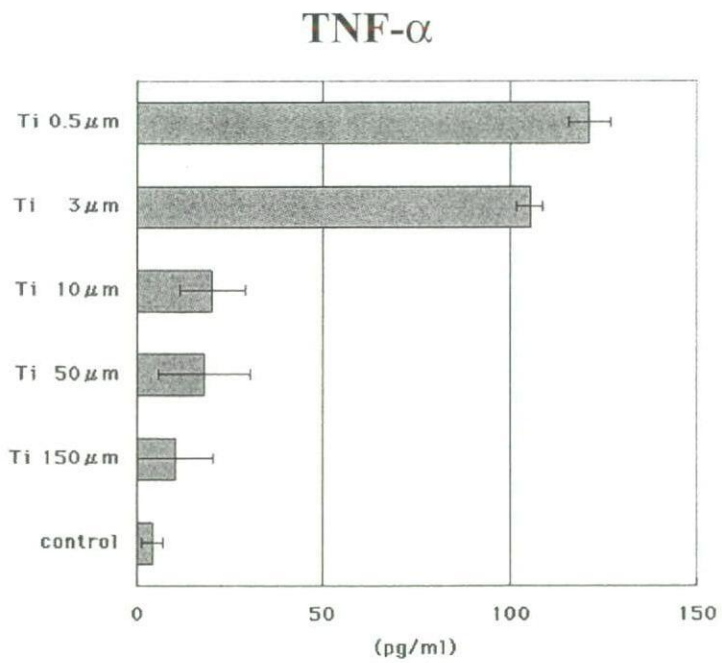

Fig. 2. Dependence of TNF-α release from human neutrophils on Ti particle size [1]

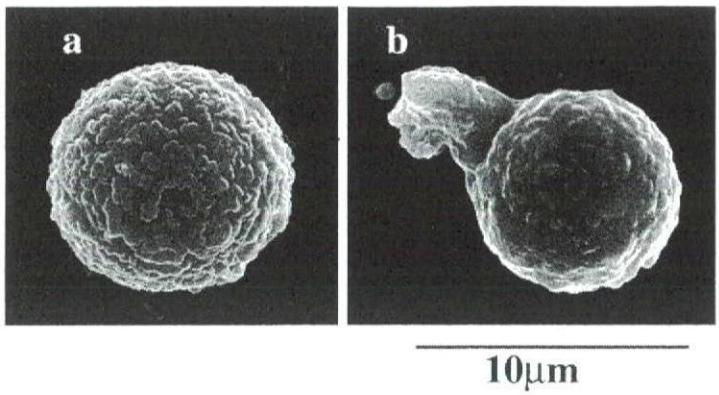

Fig. 3. SEM images of human neutrophils. **a** Control, **b** exposed to particles of Ti (500 nm) [3]

Fig. 4. Hydroxyapatite synthesized without (**a**) and with (**b**) collagen

than about 10 μm, phagocytosis was not observed. The pronounced phenomena of biochemical cell reaction for below 10 μm in Fig. 2 are closely related to the phagocytosis shown in Fig. 3.

The histological image of tissue reaction of rat to the different sizes of Ti particles showed a similar size dependence to those in vitro shown in Figs. 2 and 3.

These phenomena occur commonly in any bioactive and bioinert materials other than Ti, such as Fe and TiO_2 where particles induce non-specifically phagocytosis to cells and inflammation to tissue for the size below 10 μm, about the cell size. It is different from the usually observed toxicity due to the ionic dissolution effect in the macroscopic size [4].

Apatite formation with and without collagen

Figure 4 shows the comparison of morphology of hydroxyapatite synthesized without (a) and with (b) collagen by SEM observation. The particle size of